Available online at www.sciencedirect.com
SCIENCE DIRECT
Cement and Concrete Research 36 (2006) 189–199
Cement and Concrete Research

The role of specimen geometry and boundary conditions on stress development and cracking in the restrained ring test

Akhter B. Hossain[a,1], Jason Weiss[b,*]

[a]Department of Civil Engineering, University of South Alabama, Mobile, AL 36688, United States
[b]School of Civil Engineering, Purdue University, 550 Stadium Mall Drive, West Lafayette, IN 47907-1284, United States

Received 7 April 2004; accepted 7 June 2004

Abstract

Early-age cracking can be a significant problem in concrete pavements, floors, and bridge decks. Various test methods have been developed to assess the potential for early-age cracking, however due to the economy and simplicity of the ring test, it has become widely used. Although the ring test procedures employed by various authors are similar, they vary in terms of curing duration, specimen geometry, and boundary conditions. This paper describes an experimental study of restrained ring specimens tested using different geometries and boundary conditions. Specimen geometry was found to have a significant effect on the stress development and age of cracking in the restrained ring specimens. Specimens that shrink uniformly along the radius show the greatest variation in the age of cracking with thicker specimens cracking at a later age. Acoustic emission testing has been used to illustrate that specimen boundary condition substantially influence crack development and propagation in the restrained rings.

Keywords: Drying; Crack detection; Microcracking; Shrinkage; Residual stress

1. Background

Cement based materials experience volumetric changes as a result of moisture loss, temperature change, and chemical reactions. If restrained, these volume changes result in the development of residual tensile stresses that may be sufficient to cause cracking.

The problem of early-age cracking has been receiving significant attention recently due to the increased use of higher strength concretes that may be more susceptible to cracking [1]. Several test methods have been proposed to assess the cracking potential of concrete mixtures [2–4] including linear specimen geometries [5–8] that use either 'passive-restraint' through a steel frame [5,9,10] or 'active-restraint' from a hydraulic or electrical actuator [5–7]. The linear specimen geometry has the advantage that the interpretation of data is relatively straightforward. As a result, the linear specimens have been used in many laboratory studies. However, these test methods have not been widely used for quality control procedures due to the high cost of these frames and difficulties associated with providing sufficient end restraint [4,6].

The restrained ring-test has become more widely used as a quality control test for assessing the shrinkage cracking potential of concrete mixtures. The ring-test is economical, simple to perform, and does not pose difficulties in providing sufficient end restraint. In the ring test, a concrete annulus is cast around a steel ring. If unrestrained (i.e., no steel ring), the concrete would shrink, however, the steel ring prevents (restrains) this movement resulting in the development of tensile stresses.

Because of its simplicity and versatility, AASHTO has recommended a version of the ring test as a standard test method that can be used for assessing cracking potential of various concrete mixtures [11]. It should be noted, however, that in addition to the AASHTO standard ring, many researchers have used ring specimens with other geometries

* Corresponding author. Tel.: +1 765 494 2215; fax: +1 765 496 1364.
E-mail addresses: hossaina@jaguar1.usouthal.edu (A.B. Hossain), wjweiss@ecn.purdue.edu (J. Weiss).
[1] Tel.: +1 251 460 7438; fax: +1 251 461 1400.

0008-8846/$ - see front matter © 2005 Elsevier Ltd. All rights reserved.
doi:10.1016/j.cemconres.2004.06.043

[3]. Though the procedure of using a steel ring to resist shrinkage is similar in each of these approaches; specimen dimensions, boundary conditions, and data interpretation have been varied. AASHTO recommends a fixed geometry that allows drying from the outer circumference. This results in a complex stress field that varies its shape over time due to the presence of moisture gradients [3,27]. To overcome this difficulty, it has been suggested that the rings be allowed to dry from top and bottom [19]. Through this simple change in boundary conditions, the moisture loss becomes uniform along the radius of the specimen. Analytical expressions for thick walled cylinders were developed to calculate the actual residual stresses that develop in restrained ring specimens when the specimens undergo uniform drying shrinkage in the radial direction (i.e., drying for the top and bottom). This solution could also be used to approximate rings that dry from the circumference if the moisture gradient effect is assumed to be negligible (i.e., in the case of a very thin concrete ring). However, it should be noted that aggregate size frequently restricts how thin the ring of concrete can be made. Consequently, this approximation may not be applied for materials with realistic aggregate sizes.

2. Research synopsis

This paper compares the behavior of rings having two different boundary conditions: (1) drying from the top and bottom of the ring and (2) drying from the outer circumference of the ring. The ring geometry and the thickness of the steel ring were also varied in this investigation. The strain that developed in the steel ring was measured and the age of cracking was determined to better quantify the effects of these two boundary conditions in the restrained concrete rings. An analytical expression has been used to describe the interface pressure that develops between the concrete and steel. This interface pressure can be used to compute the maximum residual tensile stresses that develop in the concrete. Acoustic emission has been used to experimentally assess how cracks form in the rings under the different boundary conditions to illustrate the type of failure criteria that should be used for modeling.

3. Experimental program

To describe the influence of boundary conditions on the drying behavior and stress development, restrained and unrestrained specimens were prepared. The mortars were made with Type I cement (C_3S of 60%, C_2S of 13.5%, C_3A of 8.2%, Na_2O equivalent alkali content of 0.54%, the fineness of 360 m^2/kg), water-to-cement ratios (w/c) of 0.30 and 0.50, respectively, and a fine aggregate volume of 50%. After mixing, the mortar was placed in the forms (that were lined with acetate on all sides except for the surface in contact with the steel ring which was cleaned and covered with form release oil [24]). During placement, the concrete was vibrated and finished with a steel trowel to obtain a smooth surface for crack width measurement. The specimens were then placed under a plastic sheet to prevent moisture loss, and maintained at 23 °C. The specimens were demolded at an age of 24 h, sealed (as described in Sections 3.1–3.3), and placed in a 50% RH environment where they were kept for the remainder of the experiment.

Three main test methods were used to better understand how specimen geometry and boundary conditions influence stresses and the resulting cracking in restrained concrete rings:

i. free shrinkage tests,
ii. restrained ring tests, and
iii. acoustic emission tests of restrained ring specimens.

These test methods are briefly described in the following sections.

3.1. Free shrinkage tests

To better understand the effect of boundary condition on free shrinkage, two different free shrinkage tests were performed: (i) free shrinkage of unrestrained ring specimens and (ii) free shrinkage of linear specimens similar to the ASTM C-157 tests.

The unrestrained specimens were intended to mimic the restrained rings in terms of size and drying conditions (as shown in Fig. 1). The unrestrained concrete rings had an inner diameter of 300 mm (12 in.), an outer diameter of 450 mm (18 in.), and a height of 75 mm (3 in.). After demolding, the rings were sealed with aluminum tape in such a way that one ring could dry from top and bottom and the other ring could dry only from the outer circumference. It should be noted that the inner circumference of the unrestrained rings was sealed with two layers of aluminum tape to simulate the moisture conditions of the restrained

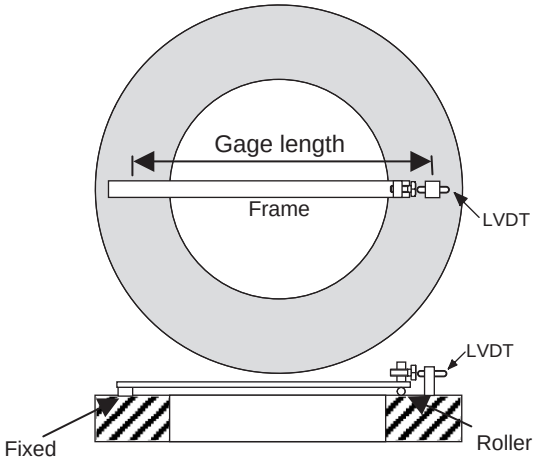

Fig. 1. Unrestrained ring specimen.

ring test. A linear variable differential transformer (LVDT) was used to measure the change in diameter of each unrestrained ring. The LVDT was mounted on a specially designed aluminum frame that was glued to the specimen surface as shown in Fig. 1. Only displacements that occurred after demolding (i.e., 24 h) could be measured using this approach.

The linear specimens were prepared following a procedure that was similar to ASTM C-157. The specimens were mortar prisms with a 75 mm (3 in.) square cross-section and 250 mm (10 in.) gage length. Unlike the specimen used in ASTM C-157, the two sides and ends of the specimens were sealed with two layers of aluminum tape to provide similar drying condition to the mortar in the restrained rings drying from the top and bottom as previously described.

3.2. Restrained ring test

Three series of restrained ring specimens were prepared to determine the effects of boundary conditions on early-age stress development and cracking in restrained rings. The degree of restraint was varied in the first series (DR) by varying the steel wall thickness. The second series was used to illustrate the response when the concrete wall thickness was varied (CWT). In the third series, the boundary condition of the specimens was varied to provide different drying directions (BC). In all series (DR, CWT, BC) the concrete rings had an inner diameter of 300 mm (12 in.) and a height of 75 mm (3 in.).

In the DR series, a constant concrete wall thickness was used by fixing the outer diameter at 450 mm (18 in.). A concrete annulus was cast around steel rings of variable wall thickness (3.1 mm (1/8 in.), 9.5 mm (3/8 in.), and 19 mm (3/4 in.), respectively) to provide a varying degree of restraint.

The rings in the CWT series had a constant steel wall thickness of 9.5 mm (3/8 in.), however, the thickness of the concrete wall was varied to include rings with a wall thickness of 37.5 mm (1.5 in.), 75 mm (3 in.), 112.5 mm (4.5 in.), and 150 mm (6 in.).

The rings in the BC series include rings similar to the rings in the DR and CWT series, however, in this series, the rings were sealed with aluminum tape to obtain two different boundary conditions (i.e., drying from the circumference and drying from the top and bottom) as shown in Fig. 2. Table 1 provides a complete summary of the specimens that were used to study each of the variables in this investigation.

The ring test can be used to quantify stress development using the strain that develops in the steel ring [19,21]. Four strain gages were connected to each ring at mid-height and interfaced with a data acquisition system in a half-bridge configuration. It should be noted that strain data were collected at 10 min intervals from approximately 30 min after the water came in contact with the cement. This was done to capture the early-age strain that developed (i.e., during the first 24 h). The specimens were sealed for the first 24 h to prevent moisture loss.

3.3. Acoustic emission test of the restrained rings

Acoustic emission testing was used to investigate the development and propagation of cracks in the restrained ring specimens under the two different drying boundary conditions (i.e., (1) circumferential drying and (2) uniform radial drying or drying from the top and bottom).

Acoustic emission is a non-destructive test method which can be used to detect cracking in concrete [12,13,19]. Acoustic emission uses piezoelectric sensors to detect sound

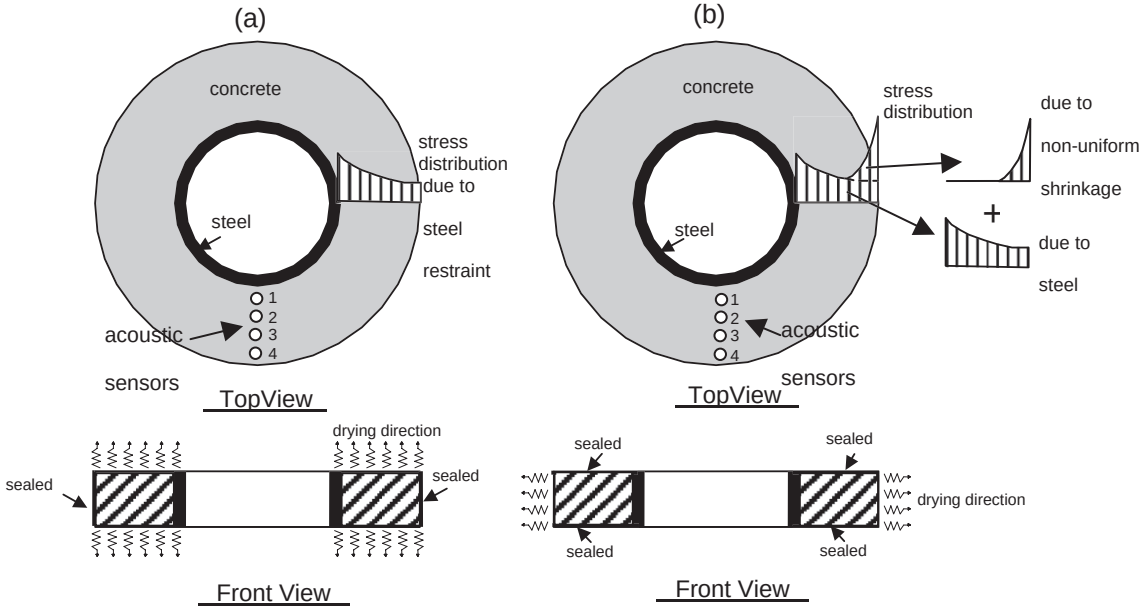

Fig. 2. Restrained ring specimens.

Table 1
Variables considered in this study

Steel wall	Concrete wall	Drying direction	
Thickness (mm)	Thickness (mm)	Circumferential	Top and bottom
Unrestrained ring specimens (0.3 and 0.5 w/c)			
–	75	√	–
–	75	–	√
Restrained ring specimens: DR and BC series (0.3 and 0.5 w/c)			
3.1	75	√	–
9.5	75	√	–
19.0	75	√	–
3.1	75	–	√
9.5	75	–	√
19.0	75	–	√
Restrained ring specimens: CWT and BC series (0.3 and 0.5 w/c)			
9.5	37.5	√	–
9.5	75	√	–
9.5	112.5	√	–
9.5	150	√	–
9.5	37.5	–	√
9.5	75	–	√
9.5	112.5	–	√
9.5	150	–	√
AE ring specimens (0.5 w/c)			
19.0	112.5	√	–
19.0	112.5	–	√

waves that are generated by local disturbances (i.e., micro and macrocracking) that occur within a material. Even though the major sources of disturbance in this study are believed to be microcracks, it should be remembered that acoustic events may be generated by other sources. The piezoelectric sensors are coupled with the surface using vacuum grease. These sensors detect displacements caused by the internal disturbances that are measured in terms of voltage. When the wave caused by the internal disturbances exceeds a certain threshold, an event (or hit) is generated. This wave has a certain amplitude (i.e., maximum voltage or corresponding sound) and a duration when the amplitude of the wave stays above a certain threshold. In this paper, only events greater than 40 dB were recorded to minimize background noise. For further details on acoustic emission, the reader is referred to recent review articles by Mindess [14] and Scott [15].

Although there are several ways to describe an acoustic event, recent research has shown that acoustic energy may provide a useful method to detect and quantify an event [16–19]. The acoustic energy is defined in this paper as the absolute value of the area under the waveform. Recent research has suggested that acoustic energy may be particularly useful since it may be directly related to fracture energy [15,16,20].

The ring specimens that were used for acoustic emission testing had a concrete wall thickness of 112.5 mm (4.5 in.). The rings were prepared using 0.50 w/c mortar that was cast around a 19 mm (3/4 in.) thick steel ring. After 24 h, the rings were demolded and sealed with aluminum tape to provide the necessary boundary conditions. A plastic notch 25 mm (1 in.) tall and 3.1 mm (1/8 in.) wide was placed in each specimen along the radius to create a weaker zone where the crack could be expected to occur (the net cross-section was 50 mm (2 in.)×112.5 mm (4.5 in.)). The introduction of the weak zone enabled the acoustic emission sensors to be located near the crack to provide the best measurement of acoustic activity.

A Vallen AMSY4 system was used to monitor the acoustic activity in each specimen. Four 375 kHz wide band sensors were attached to the upper surface of each ring using vacuum grease as a coupling agent. In the ring that was allowed to dry from the outer circumference, the sensors were attached to the top surface of the ring directly above the notch. In the ring that was allowed to dry from the top and bottom, the sensors were not placed directly above the notch and were shifted slightly (25 mm) to allow drying. Sensor 1 was placed nearest to the steel ring and Sensor 4 was placed close to the outer circumference of the concrete ring. Sensors 2 and 3 were placed in between sensors 1 and 4 as shown in Fig. 2.

4. Experimental results

The results of this study have been divided into the following four sections: (i) free shrinkage of the unrestrained ring and linear specimens, (ii) stress development in the restrained ring specimens, (iii) age of cracking in the restrained ring specimens, and (iv) crack development and propagation in the restrained ring specimens.

4.1. Free shrinkage of the unrestrained ring and linear specimens

Free shrinkage measurements taken from the linear specimens and the unrestrained rings were compared as shown in Fig. 3. The diametric deformation of the ring (measured from the LVDT) was converted to an equivalent free shrinkage strain using the following equation [19]:

$$\varepsilon_{SH} = \frac{U_{SH-D}}{D_{LVDT}} \quad (1)$$

where ε_{SH} is the free shrinkage (negative values correspond to shrinkage), U_{SH-D} is the change in diameter (as measured from the LVDT where a negative sign corresponds to a reduction in diameter), and D_{LVDT} is the diameter of the concrete ring over which the LVDT is acting.

It was observed that for both the w/c=0.30 and w/c=0.50 mixtures the free shrinkage of the unrestrained ring specimens drying from top and bottom is higher than that of the specimens drying from the outer circumference. This can be explained in part by the fact that the unrestrained ring specimen that is allowed to dry from top and bottom of the

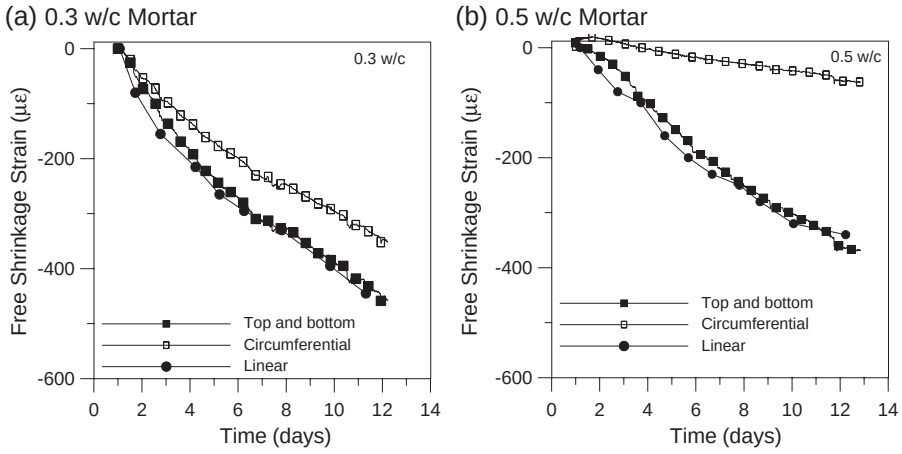

Fig. 3. Free shrinkage results.

ring has a higher exposed surface-to-volume ratio (s/v) than the specimen that dries from the outer circumference. For example, the rings with an outer diameter of 450 mm (18 in.) have an s/v of 0.0267 mm^{-1} when drying from the top and bottom and 0.0133 mm^{-1} when drying from the circumference. It should be remembered at this point that the surface to volume ratio (s/v) of specimens has significant influence on the rate of free shrinkage [21,22]. It was also observed that the specimens with lower water-to-cement ratio (w/c) demonstrated more similarity between the circumferential and uniform radial drying (drying from the top and bottom). This is likely due to the fact that, in the lower w/c specimens, a higher fraction of the total shrinkage may be due to self-desiccation (i.e., autogenous shrinkage) that occurs more uniformly throughout the specimens (i.e., more uniformly along the radial direction).

It is also interesting to observe from Fig. 3 that the linear specimens that were allowed to dry from the top and bottom demonstrated a free shrinkage that is similar to the unrestrained rings that were permitted to dry from the top and bottom. This can be explained by the fact that the linear specimens and the unrestrained rings that dry from the top and bottom have a similar exposed surface-to-volume ratio (s/v) and cross-sectional geometry.

4.2. Stress development in the restrained ring specimens

Previous studies [4,23–27] have used various techniques to quantify the results of the restrained ring test. Some studies have used the strain measured on the steel ring or simply the age of cracking to describe how various materials compare to one another. To overcome these limitations, an expression was developed [24–26] to convert the strains that are measured in the steel ring to the maximum residual tensile stresses that develop in the concrete. These residual stresses can then be related to a tensile strength or fracture mechanics failure criterion.

To convert the strains in the steel to stresses in the concrete, the concrete cylinder can be idealized as being pressurized at the inner surface and steel cylinder pressurized with an equal and opposite pressure at its outer surface with a fictitious interface pressure. The fictitious interface pressure ($p_{residual}$) that is required to generate a strain that is equivalent to the measured strain in the steel (ε_{Steel}) can be determined using the following equation [24]:

$$p_{residual}(t) = -\varepsilon_{Steel}(t)|_{r=R_{IS}} \cdot E_S \cdot \frac{\left(R_{OS}^2 - R_{IS}^2\right)}{2R_{OS}^2} \quad (2)$$

where R_{IS} and R_{OS} are the inner and outer radius of the steel ring, respectively, and v_S and E_S are the Poisson's ratio and elastic modulus of the steel, respectively. Eq. (2) illustrates that the interface pressure can be determined simply by using the steel material properties, geometry of the steel ring, and average strain that is measured at the inner radius of the steel using the electrical resistance strain gages.

Once the interface pressure is obtained, the maximum residual stress ($\sigma_{Actual-Max}$) that develops in concrete ring can be obtained using the following relationship.

$$\sigma_{Actual-Max}(t) = -\varepsilon_{Steel}(t)|r = R_{IS} \cdot E_S \cdot \frac{\left(R_{OS}^2 - R_{IS}^2\right)}{2R_{OS}^2} \cdot \frac{R_{OS}^2 + R_{OC}^2}{R_{OC}^2 - R_{OS}^2} \quad (3)$$

At this time, it should be noted that Eq. (3) is only truly valid when shrinkage occurs uniformly along the radius of the specimen. For specimens drying only from the outer circumference, the stress field is more complicated [27] as described in Fig. 2.

Figs. 4 and 5 show the results of the restrained ring tests for the 0.30 and 0.50 water-to-cement ratio (w/c) mortar specimens tested in this study. Fig. 4 shows the influence of the thickness of the steel ring (or the degree of restraint) on the interface pressure that develops between the steel and the concrete rings. The interface pressure and residual stress that developed in the 9.5 mm (3/8 in.) and 19 mm (3/4 in.) steel wall thickness specimens were generally similar (Fig. 4a–f), however, the interface pressure and the residual stress

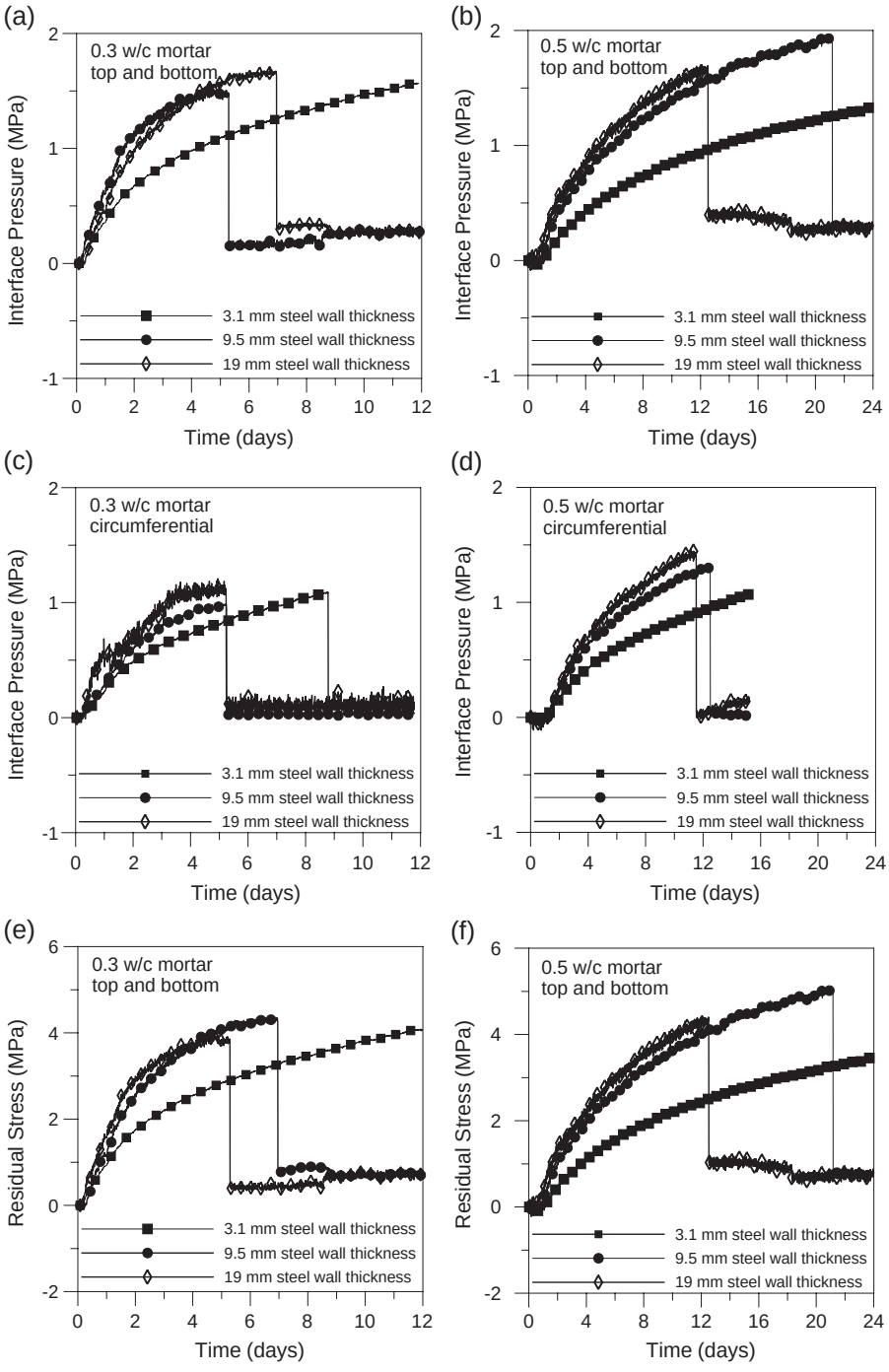

Fig. 4. Influence of steel ring thickness on the interface pressure and residual stress.

that developed in the 3.1 mm (1/8 in.) wall thickness specimen were slightly lower. This may be due to the fact that the 3.1 mm (1/8 in.) wall may be somewhat more flexible in the Z direction. Therefore, the concrete may not result in a uniform deformation of the inner steel ring along its height (Z direction) and as a result, the strain measured at the mid-height of the ring may be lower than the strain that develops at the top and bottom of the ring. Further testing is needed to verify whether this hypothesis is true. In general, it can be seen, however, that the rings with a lower thickness show a similar or slightly lower stress.

It can be noticed that the specimens which were permitted to dry from the top and bottom (Fig. 4a,b) developed a higher interface pressure than the specimens that dried only from the outer circumference (Fig. 4c,d). This may be explained again by the fact that the specimens that dry from the circumference show a lower amount of shrinkage (Fig. 3).

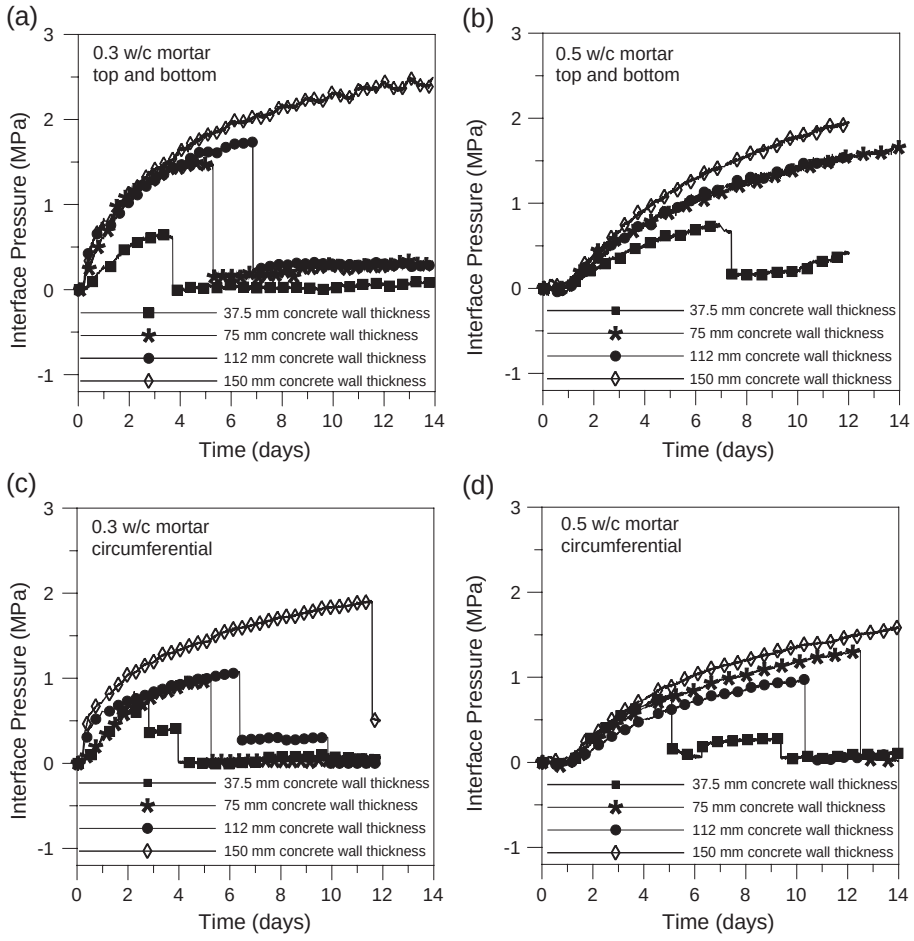

Fig. 5. Influence of concrete wall thickness on the interface pressure.

Fig. 5 illustrates the influence of the concrete wall thickness on the interface pressure that developed in the test specimens that dried from the top and bottom as well as rings that dried from the circumference. It can be seen that the direction of drying had a pronounced effect on the interface pressure that developed between the concrete and the steel ring. In general, the specimens that were permitted to dry from the top and bottom demonstrated higher interface pressures than the specimens that were drying from the outer circumference, even though they had similar restraint and specimen dimensions. The rings that dried from the outer edge demonstrated a lower level of interface pressures, presumably due to the presence of moisture gradients and the lower s/v that caused the specimen to shrink more slowly. The specimens with a 37.5 mm wall thickness showed similar interface pressures for both drying directions. This can be explained by the fact that the ring specimens with 37.5 mm concrete wall thicknesses had similar exposed s/v for both drying directions. As a result, they demonstrated a similar level of interface pressure.

It can be noticed that there was generally not a dramatic difference between the maximum stresses that developed in the concrete rings with different concrete wall thicknesses. In cases where a difference was noticed, the thicker rings developed a slightly higher interface pressure.

4.3. Age of cracking of the restrained ring specimens

The abrupt drop in interface pressures in Figs. 4 and 5 corresponds to age at which a visible crack developed in the restrained ring specimens. Fig. 6 provides a picture of a typical crack that developed in the restrained ring specimen with a 9.5 mm steel wall thickness, 75 mm concrete wall thickness, w/c of 0.50, and drying from top and bottom. The width of the crack at 35 days was 0.75 mm while the specimen that dried from circumference had a crack that was slightly larger (0.85 mm). It should be noted that the crack develops and opens relatively quickly, however, approximately 7–10 days after the crack formed, the width of the crack stabilized and did not continue to grow wider [3]. Similar information on crack width development has been reported for a wide range of concrete strengths [30]. In addition, the information from the instrumented restrained ring test (using strain gages) has recently been used to determine the crack width from the strain measurements in the ring [29,31]. It should be noted, however, that the ring test primarily provides information about the age of visible

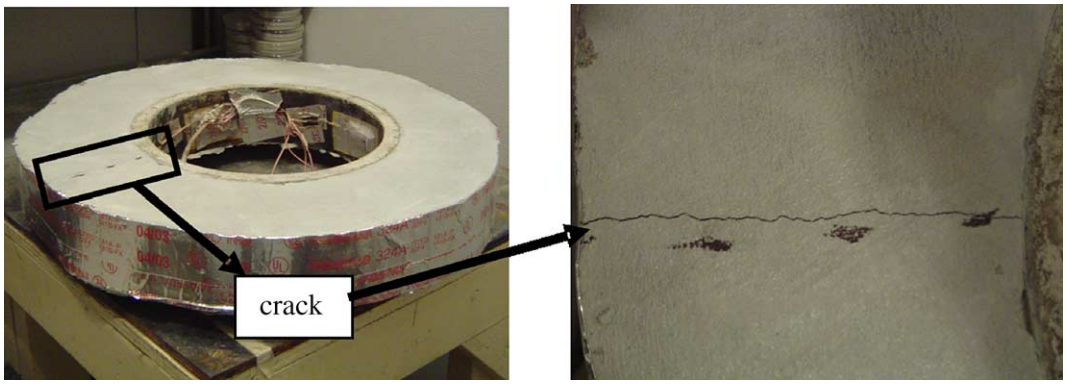

Fig. 6. Crack in restrained ring specimen drying from the top and bottom.

crack development and does not directly describe the development of microcracking or potential for healing. For information on microcrack development, additional experimental procedures are needed such as the use of acoustic emission [18–20,28,29].

Fig. 7 compares the age of visible cracking (i.e., abrupt strain drop) in the restrained ring specimens considering different geometry and boundary conditions. It is evident from Fig. 7a and b that the steel wall thickness greatly affects the age of cracking. The ring specimens with thicker steel rings crack earlier than the specimens with thinner steel ring (if the concrete wall thickness is same). For example, the mortar specimens (0.30 w/c) with a 75 mm concrete wall thickness that were allowed to dry from the top and bottom and were cast around the 18.75 mm (3/4 in.) steel ring cracked at an age of 5.3 days, while the ring that was cast around 9.38 mm (3/8 in.) steel ring cracked at 7.0 days, and the ring that was cast around 3.13 mm (1/8 in.) steel ring cracked at 13.0 days. A similar phenomenon was observed for specimens with different water-to-cement ratios (0.5) and boundary conditions. This implies that the thicker steel rings provide a higher degree of restraint which causes more damage [19] and a greater potential for cracking to develop.

Fig. 7c and d show the influence of concrete wall thickness on the age of cracking. It has been observed that rings with a thicker concrete wall crack later (if the steel wall thickness is kept constant). For example, the 0.30 w/c mortar specimens that dry from the top and bottom and have wall thicknesses of 37.5 mm (1.5 in.), 75 mm (3 in.), 112.5

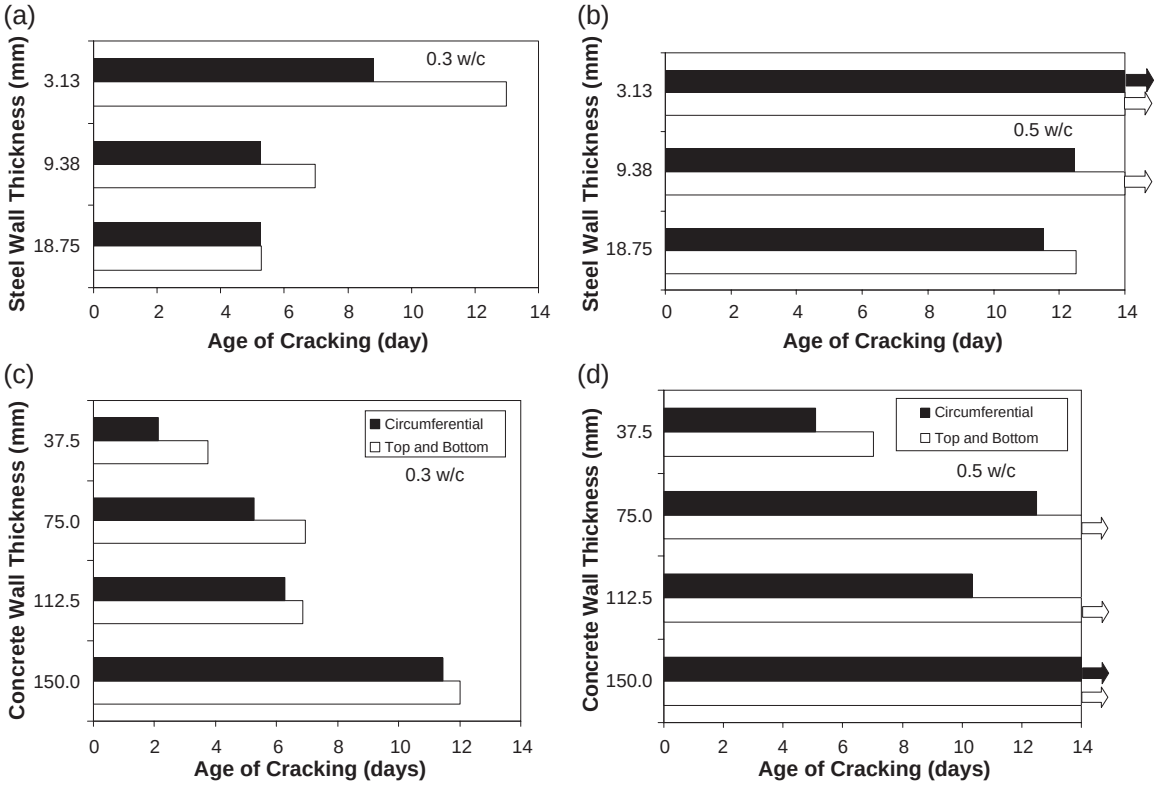

Fig. 7. Age of cracking of restrained ring specimens.

mm (4.5 in.), and 150 mm (6 in.) crack at 3.7 day, 6.9 day, 6.8 day, and 12.0 days, respectively. Similarly, the 0.30 w/c ratio specimens that dry from the outer edge crack at 2.1 day, 5.3 day, 6.3 day, and 11.5 day, respectively. This can be explained by the fact that the thicker specimens are less sensitive to the development of a similar sized initial crack [17]. This implies that the crack driving energy (the energy supplied to grow the crack) is lower for the thicker specimens which require a higher stress level to cause a crack to develop.

Fig. 7 illustrates that the restrained ring specimens that dry from the outer circumferences always crack earlier than the rings that dry from the top and bottom. It should be noted that, in this paper, the restrained specimens that dry from the outer circumference always have a concrete wall thickness that is equivalent to or greater than half the height of the ring specimen (i.e., 37.5 mm in this case). This implies that the exposed s/v is always (in this paper) greater for specimens that dry from the top and bottom and consequently these specimens should shrink faster. Despite this fact, the specimens that dry from the outer circumference cracked first which is likely due to the increased stress level that develops along the outer radius of the ring due to the presence of the moisture gradient [27] as shown in Fig. 2. As a result, it has been proposed [27] that the crack may actually initiate at the outer edge and propagate towards the inner radius. While this may appear logical, it has a significant impact on the failure theories that should be used to describe the failure of the ring since theories that are based on the conventional stress analysis consider the stress to be highest at the inner surface. Therefore, the conventional stress analysis based on the internal pressure would not be correct for the rings drying from the outer circumference due to the gradient effects. This hypothesis has been experimentally assessed and verified in the following section using acoustic emission.

For the case of the specimens that dry from the top and bottom, a more conventional stress field develops throughout the radius that varies as $1/r^2$ (as shown in Fig. 2) due to the restraint that is provided by the steel ring [27]; therefore, a conventional stress analysis and fracture failure criterion still appears appropriate.

4.4. Crack development and propagation in the restrained ring specimens using acoustic emission

In addition to the free shrinkage measurements and restrained shrinkage tests, acoustic activity was measured in the restrained ring specimens to assess how cracks develop in these specimens. Although several parameters can be used to describe acoustic activity, this paper uses acoustic energy since it provides a method to detect and quantify damage. Previous research [28] has shown that the acoustic energy release rate (the time dependent derivative of acoustic energy) can be used to describe the development and propagation of cracks in the restrained concrete specimens. Fig. 8 compares the development of interface pressure and acoustic energy release rate for the restrained mortar rings. Initially, a relatively constant rate of acoustic energy is released with small peaks that appear to correspond with changes in the rate of interfacial pressure development (Fig. 8a). At these early ages, a gradual increase in interface pressure is observed in the specimens. When the rate of acoustic energy increases, stable microcracks are believed to develop and the rate of interface pressure begins to level off. After the initial stress development period, the interface pressure becomes almost constant; however, an increase in AE release rate is noticed. During this period, it is believed that the microcracks begin to localize to form a single crack. It is believed that as soon as the crack reaches a critical length, the interface pressures show abrupt downward jump while the AE release rate curves show a sudden increase which would be consistent with the unstable propagation of a single crack. This is the time when a visible crack is formed.

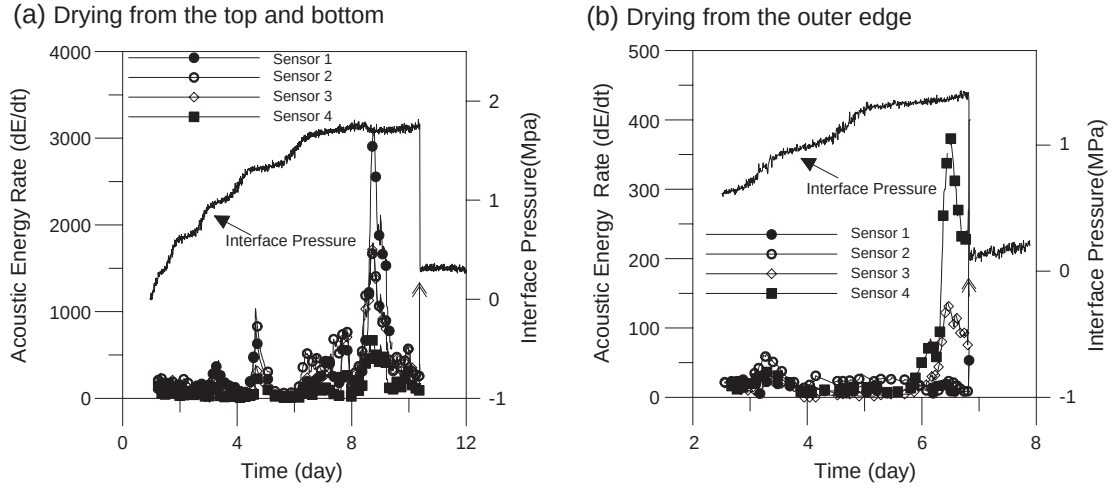

Fig. 8. Acoustic energy release rates.

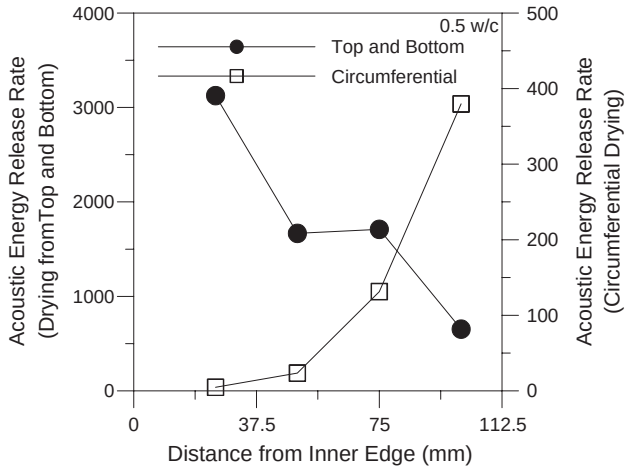

Fig. 9. Acoustic energy release rates (determined at the maximum energy release rate that occurs before visible cracking) as a function of the ring radius (i.e., 8.8 days for the top and bottom drying and 6.5 days for the circumferential drying specimens).

Fig. 9 shows acoustic energy release rates as measured by each of the sensors located along the radius in the restrained ring specimens around the time of unstable cracking. This test was performed for specimens with both boundary conditions (i.e., circumferential and top and bottom drying). The maximum energy release rate measured by each sensor is recorded which is believed to correlate to the time when the major crack begins to form (6.5 days for the circumferential drying and 8.8 days for the top and bottom drying). It can be observed from Fig. 9 that the specimen drying from the top and bottom shows the maximum AE release rate along the inner radius of the ring. This indicates that, in the specimens drying from the top and bottom, the major crack initiates at the inner edge and propagates towards the outer edge. This is consistent with the way in which damage has been modeled in several studies [17,24] based on standard elastic and viscoelastic solutions that predict a higher stress at the inner surface. In the case of the restrained ring drying from the outer circumference, it has been observed that the sensor located near the outer edge of the ring demonstrated the highest AE release rate at the time of fracture. This indicates that, in the restrained ring that dries from the outer circumference, the crack initiates at the outer edge and propagates towards the inner edge. This is consistent with the idea of the maximum tensile stress developing at the outer edge due to moisture gradients as shown in Fig. 2 [27].

5. Summary

This paper demonstrates the influence of specimen geometry and boundary conditions on the stress development and age of cracking in the restrained concrete ring specimens. This study has shown that specimen geometry has a significant influence on the measurements obtained from the restrained ring test. It has been observed that the thicker steel rings provide higher degrees of restraint resulting in higher interface pressures and cracking at an earlier age. The restrained rings with a thicker concrete wall crack later since the thicker walled specimens are less sensitive to small cracks (i.e., a lower crack driving energy).

It has been observed that the specimen boundary conditions have a significant influence on the results of the restrained ring test. It has been found that the ring specimens that are allowed to dry from the top and bottom experience higher interface pressure than the specimens that are allowed to dry from the outer circumference. This can be explained by the fact that the specimens that dry from top and bottom have a higher surface to volume ratio (s/v). It has been found that despite having lower interface pressures, the rings that dry from the outer circumference crack at an earlier age than the ring specimens drying from the top and bottom. This is presumably due to a fundamental difference in how the cracks form and how failure occurs. Acoustic emission testing has shown that, in the rings that were permitted to dry from the outer circumference, the crack initiates at the outer edge and propagates towards the inner circumference while in the rings that were allowed to dry from the top and bottom, the crack begins at the inner circumference and propagates towards the outer edge.

Acknowledgements

The authors gratefully acknowledge support received from the Center for Advanced Cement-Based Materials and the National Science Foundation (NSF). This material is based in part on work supported by the NSF Grant No. 0134272: a CAREER AWARD granted to the second author. This work was conducted in the Charles Pankow Concrete Materials Laboratory at Purdue University; as such the authors gratefully acknowledge the support which has made this laboratory and its operation possible.

References

[1] American Concrete Institute – 189, High Performance Concrete, ACI, Detroit, 1999.
[2] A. Bentur, Chapter 6.5: Early-age cracking tests, RILEM State of the Art Report – Early Age Cracking in Cementitious Systems, 2002.
[3] M. Grysbowski, S.P. Shah, Shrinkage cracking of fiber reinforced concrete, ACI Materials Journal 87 (2) (1990) 138–148.
[4] W.J. Weiss, W. Yang, S.P. Shah, Shrinkage cracking of restrained concrete slabs, ASCE Journal of Engineering Mechanics 124 (7) (1998) 765–774.
[5] K. Kovler, Testing system for determining the mechanical behavior of early age concrete under restrained and free uniaxial shrinkage, Materials and Structures, vol. 27 (170), RILEM, London, UK, 1994, pp. 324–330.
[6] S. Altoubat, D.A. Lange, Creep, shrinkage, and cracking of early age concrete, ACI Materials Journal 98 (4) (2001) 323–331.

[7] G. Toma, M. Pigeon, J. Marchand, B.L. Bercelo, Early-age autogenous restrained shrinkage: stress build up and relaxation, in: B. Persson, G. Fagerlund (Eds.), Self-desiccation and its Importance in Concrete Technology, Lund Sweden, 1999, pp. 61–72.
[8] K. van Breugel, S.J. Lokhorst, Stress-based crack criterion as a basis for the prevention of through cracks in concrete structures at early-ages, in: K. Kovler, A. Bentur (Eds.), RILEM International Conference on Early-age Cracking in Cementitous Systems (EAC'01), Haifa Israel, 2001, pp. 145–158.
[9] A.M. Parilee, M. Buil, J.J. Serrano, Effect of fiber addition on the autogenous shrinkage of silica fume concrete, ACI Materials Journal 86 (2) (1989) 139–144.
[10] S. Vepakomma, D. Zollinger, J.H. Jeong, Characterization of cracking restraint at sawcut joints using the German Cracking frame, 81st Annual Meeting of the Transportation Research Board, Washington, DC, 2002.
[11] Standard practice for estimating the crack tendency of concrete, AASHTO Designation PP-34-89, pp. 179–182.
[12] Z. Li, K. Kulkarni, S.P. Shah, New test method for determining post-peak response of concrete specimens under uniaxial tension, Experimental Mechanics 33 (1993) 181–188.
[13] P. Rossi, N. Godart, J.L. Robert, J.P. Gervais, D. Bruhat, Investigation of the basic creep of concrete by acoustic emission, Materials and Structures 27 (1994) 510–514.
[14] S. Mindess, Acoustic emission methods, (Chapter 14), in: V.M. Carino, N.J. Carino (Eds.), CRC Handbook on Non Destructive Testing of Concrete, CRC Press, Boca Raton, FL, 1991.
[15] I.G. Scott, Basic Acoustic Emission, Gordon and Breach Science Publishers, New York, 1991.
[16] E. Landis, L. Ballion, Experiments to relate acoustic energy to fracture energy of concrete, Journal of Engineering Mechanics 128 (6) (2002 June) 698–702.
[17] W.J. Weiss, W. Yang, S.P. Shah, Influence of specimen size and geometry on shrinkage cracking, Journal of Engineering Mechanics, ASCE 126 (1) (2000) 93–110.
[18] T. Chariton, W.J. Weiss, Using acoustic emission to monitor damage development in mortars restrained from volumetric changes, Concrete: Material Science to Application—a tribute to Surendra P. Shah, ACI International, SP-206, 2002, pp. 205–217.
[19] A. Hossain, B. Pease, W.J. Weiss, Quantifying early-age stress development and cracking in low W/C concrete using the restrained ring test with acoustic emission, transportation research record, Concrete Materials and Construction 1834 (2003) 24–33.
[20] S. Puri, Assessing the development of localized damage in concrete under compressive loading using acoustic emission, MSCE thesis, School of Civil Engineering, Purdue University, West Lafayette IN, May 2003, p. 111.
[21] J.A. Almudaiheem, W. Hansen, Effect of specimen size and shape on drying shrinkage, ACI Materials Journal 84 (2) (1987) 130–135.
[22] A.M. Neville, Properties of Concrete, Addison Wesley Longman Limited, Essex, England, 1996.
[23] Wiss, Janney, Elstner Associates, Inc., Transverse cracking in newly constructed bridge decks, NCHRP Project 12–37, 1995.
[24] A. Hossain, J. Weiss, Assessing residual stress development and stress relaxation in restrained concrete ring specimens, Cement and Concrete Composites 26 (5) (2004) 531–540.
[25] W.J. Weiss, S. Furguson, Restrained shrinkage testing: the impact of specimen geometry on quality control testing for material performance assessment, in: F.J. Ulm, Z.P. Bazant, F.H. Wittman (Eds.), Concreep 6: Creep, Shrinkage, and Curability Mechanic of Concrete and Other Quasi-brittle Materials, Elsevier, Cambridge, MA, 2001, pp. 645–651.
[26] E.K. Attiogbe, H.T. See, M.A. Miltenberger, Tensile creeep in restrained shrinkage, concreep 6: creep, shrinkage, and curability mechanic of concrete and other quasi-brittle materials, in: F.J. Ulm, Z.P. Bazant, F.H. Wittman (Eds.), Concreep 6: Creep, Shrinkage, and Durability Mechanics of Concrete and Other Quasi-Brittle Materials, Elsevier, Cambridge, MA, 2001, pp. 651–656.
[27] W.J. Weiss, S.P. Shah, Restrained shrinkage cracking: the role of shrinkage reducing admixtures and specimen geometry, Materials and Structures 35 (2002) 85–91.
[28] B. Kim, W.J. Weiss, Using acoustic emission to quantify damage in restrained fiber reinforced cement mortars, Cement and Concrete Research 33 (11) (2003) 207–214.
[29] H.R. Shah, A.B. Hossain, G. Mazzotta, W.J. Weiss, Time dependent fracture in restrained concrete: the influence of notches and fibers, in: D.A. Lange, K.L. Scrivener, J. Marchand (Eds.), Advances in Cement and Concrete: Volume Change, Cracking and Durability, Engineering Conferences International, Copper Mountain USA., Aug. 10–14, 2003, pp. 269–280.
[30] K. Wiegrink, S. Marikunte, S.P. Shah, Shrinkage cracking of high strength concrete, ACI Materials Journal 93 (5) (1996) 409–415.
[31] Shah, H.R., Quantifying the role of steel fiber reinforcement in mitigating restrained shrinkage cracking in concrete, MSCE thesis, School of Civil Engineering Purdue University, 2004.